Understanding Catalytic Specificity in Alanine Racemase from Quantum Mechanical and Molecular Mechanical Simulations of the Arginine 219 Mutant

ARTICLE *in* BIOCHEMISTRY · MAY 2010

Impact Factor: 3.02 · DOI: 10.1021/bi1002629 · Source: PubMed

2 AUTHORS, INCLUDING:

Dan Thomas Major
Bar Ilan University
75 PUBLICATIONS **1,321** CITATIONS

BIOCHEMISTRY
including biophysical chemistry & molecular biology
Article

Biochemistry **2010,** *49,* 3957–3964 3957
DOI: 10.1021/bi1002629

Understanding Catalytic Specificity in Alanine Racemase from Quantum Mechanical and Molecular Mechanical Simulations of the Arginine 219 Mutant†

Amir Rubinstein and Dan Thomas Major*

Department of Chemistry and Lise Meitner-Minerva Center of Computational Quantum Chemistry, Bar-Ilan University, Ramat-Gan 52900, Israel

Received February 21, 2010; Revised Manuscript Received March 29, 2010

ABSTRACT: Alanine racemase (AlaR) catalyzes the interconversion between L-Ala and D-Ala with the aid of the cofactor pyridoxal 5′-phosphate (PLP). The pyridine nitrogen in PLP in the wild-type enzyme is unprotonated due to interaction with Arg219, a rare feature among PLP-dependent enzymes. Herein, we performed combined quantum mechanics and molecular mechanics molecular dynamics simulations to study the Arg219Glu mutant AlaR. In this form of the enzyme, the PLP-pyridine nitrogen is protonated. This study suggests that the catalytic effect in the Arg219Glu mutant enzyme is due to a combined solvent and inherent stabilizing effect of the protonated cofactor, in contrast to the wild-type enzyme where the catalytic effect may be ascribed to solvent effects alone. Furthermore, we find that the quinonoid intermediate is greatly stabilized in the mutant enzyme, opening the possibility for side reactions such as transamination. We show that a computed 1,3-proton transfer in PLP due to the catalytic Lys39 is a feasible side reaction en route to transamination.

Nature predominantly employs L-amino acids for cell functioning. However, D-amino acids are crucial for the survival of bacteria which employ the D-isomers as principle building blocks in the peptidoglycan layers (*1*). The peptidoglycan is a strong and flexible polymer that encapsulates the cell wall providing bacteria with resilience, counteracting the cell's osmotic pressure. The principle D-amino acids used by bacteria are D-Ala and D-Glu. Additional D-amino acids such as D-Met, D-Leu, D-Tyr, and D-Phe have been found to regulate peptidoglycan synthesis (*2*). Additionally, D-amino acids have been found to modulate brain function in mammals (*3*).

Alanine racemase (AlaR)[1] catalyzes the interconversion between L-Ala and D-Ala in the presence of the cofactor pyridoxal 5′-phosphate (PLP) (Scheme 1). AlaR has been isolated from bacteria such as *Pseudomonas aeruginosa* (*4*, *5*), *Salmonella typhimurium* (*6*, *7*), and *Bacillus stearothermophilus* (*8*−*10*). Because of the importance of AlaR in bacterial synthesis, this enzyme presents an important antibiotic target. At present, most studies of AlaR have focused on enzyme inhibition and several potent inhibitors have been found (*11*). The mechanistic aspects of the racemization reaction have been studied extensively with both experimental (*9*, *10*, *12*−*20*) and theoretical tools (*21*, *22*). It has been demonstrated by mutagenesis experiments (*15*−*17*) and several crystal structures (*10*, *13*, *14*) that the catalysis is performed by the acid base pair Tyr265′ (prime indicates residues from the second subunit) and Lys39 which are located on opposite sides of the PLP-conjugated plane. The principle steps of the racemization reaction (e.g., L → D isomerization) involve (Scheme 2) (1) binding of L-Ala to the enzyme in an internal aldimine state with the PLP cofactor bound via a Schiff base to Lys39, (2) formation by L-Ala of an external aldimine with the PLP cofactor (Ala-PLP) via displacement of Lys39, (3) abstraction by Tyr265′ of a proton from L-Ala forming a quinonoid intermediate, (4) reprotonation by Lys39 to form D-Ala linked to PLP in an external aldimine form, and (5) displacement by Lys39 of D-Ala to form an internal aldimine and subsequent release of D-Ala. Mutational analysis and kinetic isotope effect measurements indicate that the proton abstraction reaction is the principle rate-limiting step (*15*−*19*). Toney and co-workers have presented a detailed free energy profile for this reaction (*19*, *20*).

An interesting feature in AlaR is the protonation state of the pyridine ring of the PLP cofactor, which has a pK_a value estimated initially to be ca. 5 (*23*, *24*) and more recently to be 5.8 (*25*). Consequently, in most PLP-dependent enzymes, the pyridine ring nitrogen is protonated due to the presence of neighboring acidic or polar amino acids. For instance, in aminotransferases, Asp or Glu interacts with the pyridinium ion (*26*), whereas in members of the tryptophan synthase family, polar residues, such as Ser or Thr, are located in the vicinity of the PLP ring heteroatom (*27*). Indeed, model computational works on PLP-dependent enzymes have typically employed a protonated PLP pyridine ring (*28*, *29*). However, in AlaR, the pyridine ring is unprotonated because of the presence of Arg219 (*13*, *19*), which has a pK_a value of ∼13 in water (*30*). The X-ray crystal structures of Ringe and co-workers described this structural feature whereby Arg219 directly donates a hydrogen bond to the pyridine nitrogen, preventing the formation of a cationic pyridinium ion (*13*). Furthermore, a quinonoid intermediate is not observed in wild-type AlaR or in the Arg219Lys and

†This work has been supported by a start-up grant from Bar-Ilan University and the Alon fellowship from the Council for Higher Education planning and budgeting committee.

*To whom correspondence should be addressed. Phone: 972-3-5317392. Fax: 972-3-7384053. E-mail: majort@mail.biu.ac.il.

[1]Abbreviations: AlaR, alanine racemase; PLP, pyridoxal 5′-phosphate; PLP(H^+), pyridine-protonated PLP; QM/MM, quantum mechanical and molecular mechanical; SRP, specific reaction parameters; WHAM, weighted histogram analysis method; MD, molecular dynamics; NQE, nuclear quantum mechanical effects; PI, path integral; PMF, potential of mean force; PMP, pyridoxamine 5′-phosphate.

Published on Web 04/15/2010

Arg219Ala mutants, whereas it is observed in the Arg219Glu mutant (*15*). Seemingly, this unusual protonation state in the wild-type enzyme plays a significant functional role. Indeed, Richard et al. found that the PLP(H^+) cofactor reduces the Cα acidity of Gly by ~12 pK_a units, i.e., from 29 to 17 (*31*, *32*). Moreover, the N-unprotonated Gly-PLP is estimated to have an intermediate value between these two. In comparison, early kinetic work of Dixon and Bruice suggested a pK_a of 12 for Ala-PLP(H^+) and a value of 14 for Ala-PLP (*23*). Model simulations of Ala and protonated and unprotonated Ala-PLP in aqueous solution suggested that the N-protonated cofactor form reduces the Ala Cα pK_a value by nearly 22 units, whereas in the unprotonated form, the pK_a is reduced by 13 units (*22*). The principle catalytic effect of Ala-PLP may be ascribed to solvation (*22*, *33*). It is assumed that in the enzyme, the unprotonated form yields an intermediate with a limited lifetime, a feature that likely aids the enzyme in avoiding side reactions (*24*).

It is of great interest to understand the difference in the mechanism of carbon acidity enhancement by the PLP cofactor in wild-type AlaR which employs an unprotonated cofactor and the Arg219Glu mutant where a protonated pyridine is present. In this paper, we compare the catalytic mechanism of Arg219Glu with wild-type AlaR and provide an atomic-level rationale for the specificity of AlaR. We employ classical molecular dynamics (MD) simulations employing a hybrid quantum mechanical and molecular mechanical (QM/MM) potential energy surface. In the following, we first describe the computational procedures used in this study, which is followed by Results and Discussion. Finally, we highlight the major findings of this study.

COMPUTATIONAL DETAILS

Model of the Solvated Enzyme−Coenzyme−Substrate Complex. The Arg219Glu mutant AlaR was prepared with a previously extensively equilibrated wild-type enzyme employed as a starting point (*22*). AlaR is a homodimer containing two domains (*13*). The N-terminal domain is composed of an eight-stranded α/β-barrel, while the C-terminal domain is characterized by α-helices and antiparallel β-sheets. The two active sites are located at the interfaces between the two subunits. In this work, we employed the structures published by Esaki et al. which were determined at 2.0 Å resolution [Protein Data Bank (PDB) entries 1L6F and 1L6G] (*10*). In these structures, AlaR forms a complex with the reaction intermediate analogues *N*-(5′-phosphopyridoxyl)-L-alanine and *N*-(5′-phosphopyridoxyl)-D-alanine, respectively. The latter structure was used to construct the external aldimine Michaelis complex of the wild-type enzyme in our study using CHARMM (*34*). We obtained the mutant enzyme by mutating Arg219 to Glu. The Arg219 side chain was manually deleted and replaced with Glu. Glu219 was oriented in a position to form an ion pair with the protonated cofactor pyridine nitrogen. The mutant enzyme was subsequently minimized and allowed to relax in the presence of the mutation as described below. It is assumed that no major changes to the active site interactions occur upon mutation. This is a reasonable assumption based on a similar type of mutation in D-amino acid transaminase (*35*). In the Glu177Lys mutant form of this enzyme, the cofactor is in a position very similar to that of the wild-type structure and the cofactor interactions are intact.

Scheme 1: External Aldimine Adduct of L-Alanine and Pyridoxal 5′-Phosphate Cofactor in Wild-Type (Ala-PLP) and Arg219Glu [Ala-PLP(H^+)] Alanine Racemase

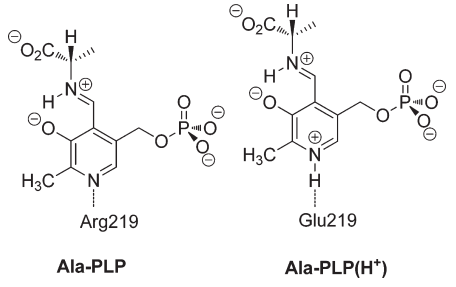

The protonation states of ionizable residues were assigned corresponding to pH 7. Interior histidines are modeled as neutral residues with the titratable hydrogen positioned at the Nδ or Nε position depending on hydrogen bonding patterns with the surrounding amino acid residues. We have treated histidine residues that are exposed to the solvent or that are forming ion pairs as protonated. The protonation state of the Ala-PLP adduct is shown in Scheme 1. Importantly, the pyridine nitrogen is treated as protonated because of the interaction with Glu219 in the mutant enzyme, which has been suggested by ^{15}N NMR experiments (*36*−*38*).

Hybrid SRP-QM/MM Potential Energy Surface. The proton transfer reactions in Arg219Glu AlaR are treated with a hybrid QM/MM potential energy surface (*39*).

$$\hat{H} = \hat{H}_{QM} + \hat{H}_{MM} + \hat{H}_{QM/MM} \quad (1)$$

The QM region is treated by a semiempirical Hamiltonian which has been optimized for enzymatic racemization reactions (*21*, *22*). Specifically, we employ the specific reaction parameter Hamiltonian AM1-SRP which was developed to treat the AlaR reaction and subsequently also employed in the study of GluR (*40*) and ProR (*33*). This Hamiltonian provides an accurate description of the proton transfer reactions in the gas phase, in solution, and in enzymes. The QM region was composed of the Ala-PLP cofactor (excluding the phosphate moiety), Tyr265′, and Lys39, as described previously (*22*). The MM region is described by the CHARMM22 (*41*) force field for the protein; the cofactor phosphate moiety is treated with the CHARMM27 force field (*42*, *43*), while water molecules are treated with the TIP3P model (*44*).

Scheme 2: Alanine Racemase Reaction Mechanism

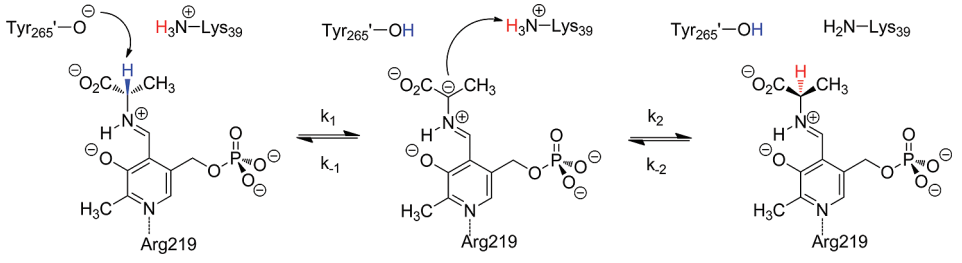

Table 1: Average Distances (Å) for Selected Hydrogen Bonding Interactions in the Michaelis Complex (L-Ala), Transition State, and Intermediate State in the Arg219Glu AlaR Mutant (L → D direction)[a]

donor		acceptor		RS[b]	TS[c]	intermediate
R136	NH1	PLP	O3A	3.86	3.92	3.48
R136	NH2	PLP	O3A	2.74	2.74	2.70
R136	NH1	PLP	OXT	3.71	3.30	2.86
H166	NE2	Y265′	OH	2.67	2.69	2.98
M312	N	PLP	O	2.68	2.71	2.67
K39	NZ	D313′	OD2	2.38	2.38	2.39
K39	NZ	Y43	OH	4.71	4.56	4.72
PLP	CA	Y265′	OH	3.11	2.62	3.29
Y265′	HH	Y265′	OH	2.60	1.41	0.98
PLP	CA	Y265′	HH	1.13	1.29	2.54
PLP	N1	E219	OE1	4.47	4.36	4.47
PLP	N1	E219	OE2	2.59	2.55	2.62

[a]The structures have been averaged over 5000 configurations. Standard deviations in the average distances are 0.10−0.30 Å. [b]Reactant state. [c]Transition state.

Table 2: Average Distances (Å) for Selected Hydrogen Bond Interactions in the Michaelis Complex (D-Ala), Transition State, and Intermediate State in the Arg219Glu AlaR Mutant (D → L direction)[a]

donor		acceptor		RS[b]	TS[c]	intermediate
R136	NH1	PLP	O3A	3.81	3.94	3.66
R136	NH2	PLP	O3A	2.76	2.80	2.75
R136	NH1	PLP	OXT	2.62	2.59	2.68
H166	NE2	Y265′	OH	2.83	2.88	3.18
M312	N	PLP	O	2.84	2.74	2.71
K39	NZ	D313′	OD2	3.32	2.66	2.37
K39	NZ	Y43	OH	3.91	4.32	4.67
PLP	CA	K39	NZ	3.48	2.71	3.30
K39	HZ3	K39	NZ	2.63	1.36	1.01
PLP	CA	K39	HZ3	1.13	1.37	2.50
PLP	N1	E219	OE1	4.44	4.15	4.50
PLP	N1	E219	OE2	2.59	2.61	2.62

[a]The structures have been averaged over 5000 configurations. Standard deviations in the average distances are 0.10−0.30 Å. [b]Reactant state. [c]Transition state.

Potential of Mean Force Simulations. The classical potential of mean force (PMF) as a function of the reaction coordinate ζ is defined as

$$W(\zeta) = -RT \ln \rho(\zeta) + C \quad (2)$$

where ρ is the unbiased probability density along the reaction coordinate ζ, R is the gas phase constant, T is the temperature, and C is a normalization constant (*45*). The reaction coordinate of the racemization step was defined as the difference between breaking the Cα−H bond and forming O−H (Tyr265′ as the base in the L-to-D conversion) or N−H (Lys39 as the base in the D-to-L isomerization) bonds. The reaction coordinate of the pretransamination 1,3-proton transfer step was defined as the difference between breaking the Cα−H bond and forming the C4′−H bond. The PMF was obtained by employing adaptive umbrella sampling MD simulations (*46*). The reaction coordinate is divided into windows that are sampled in separate simulations. A biasing, or so-called umbrella potential, is employed to improve the sampling of regions that are high in energy, yielding uniform sampling of the potential energy surface. The free energies of the separate simulation windows along the reaction coordinate are combined using the weighed histogram analysis method (WHAM) (*47*), to remove the contributions of the biasing potentials.

Stochastic boundary conditions are used here to model the active site of AlaR due to the size of the enzyme (*48*, *49*). Such boundary conditions serve as a thermal bath, preserve structural and dynamic properties of the system, and prevent the escape of water molecules from the dynamic region. The Cα atom of the Ala-PLP adduct is centered at the origin of the coordinate system, which is embedded in a sphere of water molecules with a radius of 30 Å to mimic the aqueous environment. Water molecules that are within 2.6 Å of any non-hydrogen atoms of the enzyme, substrate, and crystal waters are deleted. All protein atoms outside of the 30 Å sphere are fixed throughout the simulations. The dynamics for atoms 25−30 Å from the origin are propagated using the Langevin equation, and all atoms within 25 Å of the origin are treated by Newtonian molecular dynamics. In the Langevin region, the protein atoms are given a friction coefficient of 200 ps^{-1}, and it is set to 62 ps^{-1} for water molecules. The leapfrog integration scheme is used in all simulations with a time step of 1 fs (*50*), and the temperature of the system was set at 298 K. The electrostatic forces were shifted to zero at 14 Å, while the van der Waals interaction energy was switched to zero from 12 to 14 Å. Bond lengths involving hydrogen atoms were constrained using the SHAKE algorithm (*50*).

The system is slowly heated over the course of 25 ps, followed by equilibration for 400 ps. During the equilibration, the ion pair interaction between Glu219 and the protonated pyridine remained intact. The interaction network in the active site remained intact to within the standard deviation (Tables 1 and 2). Thereafter, the two steps of the AlaR reaction are divided into 13 windows, and the 1,3-proton transfer reaction is divided into 21 windows. Each window is further equilibrated for at least 100 ps and sampled for at least 100 ps. Sampling was continued until the PMF was invariant to within approximately ±1.0 kcal/mol, which is the expected statistical error in such simulations (*51*).

Nuclear Quantum Mechanical Effects. Nuclear quantum mechanical effects (NQE) are not included in the PMF obtained from classical MD simulations. These effects are required for the determination of accurate rate constants in proton transfer reactions. In this work, we employ bisection centroid path integral (PI) simulations to evaluate the NQE on the computed free energy barriers (*52*−*54*). In the PI simulation, we represent each quantized atom by a ring of quasi-particles or beads, wherein their geometrical center (centroid) is constrained to the classical position. Thus, for a classical configuration sampled in MD umbrella sampling simulations, PI sampling is performed to find the correction for NQE.

In this study, we use 32 beads for each of the quantized atoms (donor and acceptor heavy atoms and the transferring proton). Previous studies have shown that this treatment yields good convergence in the overall quantum corrections for model proton transfer reactions in water (*53*). For each of the reactions (wild type and mutant), 20000 configurations are extracted from the MD trajectory. For each such configuration, 10 Monte Carlo free particle sampling steps are performed.

RESULTS AND DISCUSSION

Racemization Reaction. (*i*) *Free Energy Simulations*. To study the effect of the mutation of the Arg219 residue to Glu, we computed the free energy profiles of wild-type AlaR

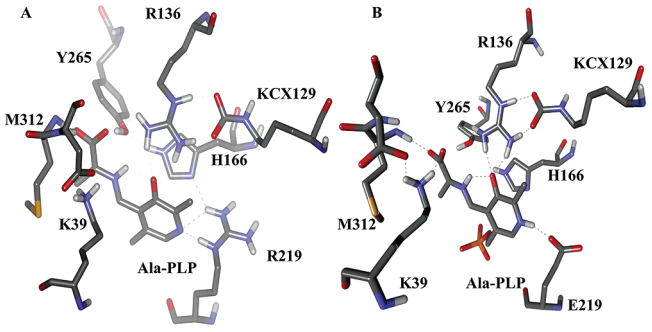

FIGURE 1: Intermediate in the racemization reaction in (A) wt-AlaR and (B) the Arg219Glu mutant.

(wt-AlaR) and the mutant enzyme from hybrid QM/MM molecular dynamics simulations. We note that the wt-AlaR PMF profile obtained here is nearly identical to the one obtained previously (*21*, *22*) and within the statistical error in the simulations.

Inspection of Figure 1A reveals that Arg219 interacts with His166's ND1 and PLP's N1, mainly via dipole−ion interactions. The mutation of Arg219 to Glu gives rise to an altered protonation state, where the PLP is protonated at the pyridine nitrogen position, N1 (Figure 1B). This is suggested by standard pK_a values of Arg, Asp (*30*), and the PLP-pyridine (*19*, *23*) as well as related ^{15}N NMR experiments (*24*, *25*, *36*−*38*). A change in the protonation state of the pyridine nitrogen has been shown to yield qualitatively different thermodynamic and kinetic properties in the aqueous solution phase (*22*, *31*). It is therefore of great interest to study these properties in mutant Arg219Glu AlaR.

The computed classical PMF for the Arg219Glu mutant AlaR reaction is depicted in Figure 2. The AlaR catalytic cycle involves two proton transfer reactions in each direction of the racemization. In the L-to-D direction, the Tyr265′ phenolate ion abstracts the Cα proton to yield a carbanion intermediate, which is followed by a proton transfer from Lys39 to form D-alanine (Scheme 2). The reaction coordinate for the first proton transfer step is defined as the difference in bond length between Cα−H and H−$O_{Tyr265'}$ bonds, while that of the second step is defined as the difference in bond length between Cα−H and H−N_{Lys39} bonds, as described in Computational Details. By this definition, the quinonoid intermediate has a reaction coordinate that is positive in the first step and negative in the second step. In constructing Figures 2−4, we shifted the reaction coordinate by approximately −1 and 1 Å for the first and second reaction steps, respectively, to display both reaction profiles in the same figure. Additionally, we set the relative free energy of the reactant state minimum of the L-Ala-PLP enzyme complex to zero and the free energies for the Ala-PLP deprotonation intermediate to be identical for both reaction steps.

The free energy profile for the Arg219Glu mutant differs considerably from the wild-type reaction profile (Figure 2). The classical PMF profile for the L → D direction suggests a barrier for the proton abstraction of L-Ala by Tyr265′ in wt-AlaR of 20.0 kcal/mol, while in the mutant form, it is 17.4 kcal/mol. This difference may be ascribed to destabilization of the phenoxide in the mutant form due to the missing interaction with Arg219 via His166 and added long-range repulsion with Glu219 (Figure 1). Addition of NQE reduces the barriers by 3.0 and 2.9 kcal/mol for wt-AlaR and the Arg219Glu mutant. This effect is largely due to the zero-point energy in the RS which is lost as the system moves to the TS (*22*). Thus, inclusion of NQE yields barriers of 17.0 and 14.5 kcal/mol for wt-AlaR and the Arg219Glu mutant,

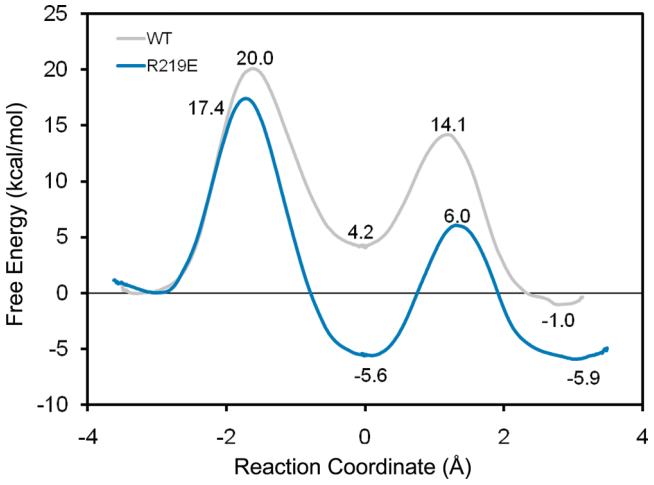

FIGURE 2: Free energy profile for the racemization in AlaR and the Arg219Glu mutant.

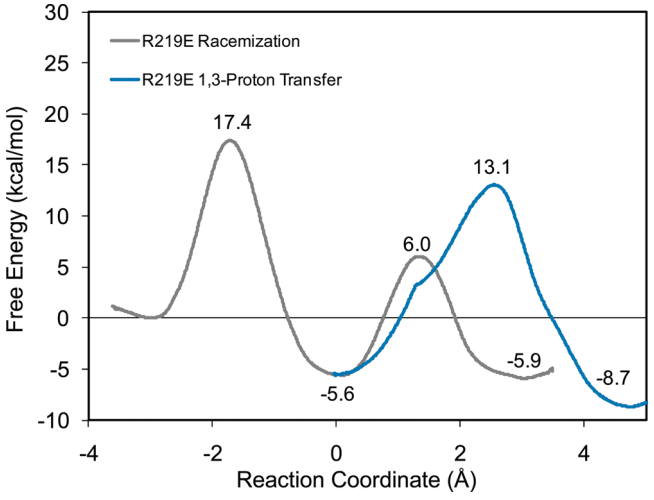

FIGURE 3: Free energy profile for the 1,3-proton transfer in the Arg219Glu mutant of AlaR.

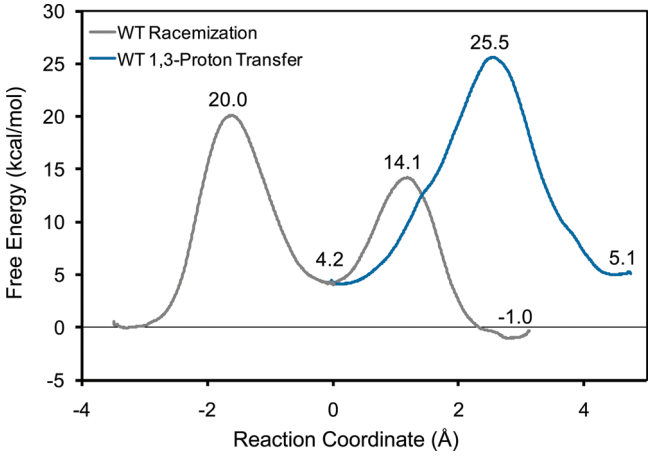

FIGURE 4: Free energy profile for the 1,3-proton transfer in wt-AlaR.

respectively. These numbers compare with values obtained from the experimental k_{cat} of 13.1 and 18.0 kcal/mol for the wild-type and mutant forms, respectively (*15*). We note that to compare directly the computed free energy barrier in the L → D direction, it is necessary to add the free energy of deprotonation of Tyr265′. This was not attempted here. Additionally, the intermediate is

more stable in the mutant enzyme which will be discussed below, resulting in an earlier transition state and concomitant stabilization of the transition state in accordance with the Hammond postulate. In wt-AlaR for the D → L direction, the classical free energy barrier to reach the intermediate is 15.1 kcal/mol, while the overall classical barrier is 21.0 kcal/mol. In the Arg219Glu mutant, the classical free energy barrier to reach the intermediate is 11.9 kcal/mol, while the overall classical barrier is 23.3 kcal/mol. Addition of NQE to the overall free energy barriers in the D → L direction yields values of 18.0 and 20.4 kcal/mol for the wild-type and mutant reactions, respectively. These numbers compare with values obtained from the experimental k_{cat} of 13.3 and 18.1 kcal/mol for the wild-type and mutant forms, respectively (*15*). The reduced barrier in the first half of the D → L reaction may be ascribed to favorable long-range interaction between the developing positive charge on the Lys39 residue and Glu219, as well as the enhanced stabilization of the intermediate. The computed shift in the overall free energy barrier in the D → L direction due to the mutation is 2.4 kcal/mol, when accounting for NQE. These computed values compare well with the experimental shift which is 4.8 kcal/mol obtained from barriers of 18.1 and 13.3 kcal/mol for the mutant and wild-type enzymes, respectively, obtained from the experimental k_{cat} values for the D → L direction (*15*). For the overall reaction in the forward direction, the reaction free energy is −5.9 kcal/mol in Arg219Glu compared to −1.0 kcal/mol in wt-AlaR. On the basis of the experimental pK_a values of the acid−base couple in wt-AlaR, Tyr265′ and Lys39, the free energy change of the overall reaction in the forward direction for the mutant, ΔG_{expt}, is expected to be close to −3.4 kcal/mol (*15*). The correlation of this value (−3.4 kcal/mol) with the calculated value (−5.9 kcal/mol) is good. The shift in the computed reaction free energy profile due to the mutation is 4.9 kcal/mol.

The PMF profile presented in Figure 2 shows that the intermediate is stabilized by −5.6 kcal/mol compared to the L-Ala state. In comparison, in wild-type AlaR, the intermediate is destabilized by 4.2 kcal/mol relative to the L-Ala state, yielding a combined stabilizing effect of 9.8 kcal/mol due to the mutation. This is a considerable effect, and the formation of a stable quinonoid is observed in our calculations on the Arg219Glu mutant, in agreement with experiment (*15*). Moreover, it seems that accumulation of the intermediate is reasonable in the D → L reaction, since the reprotonation barrier of the quinonoid intermediate by Tyr265-OH is considerable, with a value of 23.0 kcal/mol. This finding is supported by experimental evidence, in which an absorption peak at 510 nm, characteristic of a quinonoid intermediate, was observed in the D → L direction only (*15*).

The kinetic and thermodynamic properties of the Arg219Glu mutant may be compared with the results of the model reaction of N-protonated Ala-PLP [Ala-PLP(H^+)] deprotonation by phenolate in aqueous solution, which was obtained previously by free energy simulations (*22*). The free energy barrier for deprotonation of Ala-PLP(H^+) by a phenolate ion was previously found to be 22.3 kcal/mol, while the reaction free energy was 1.3 kcal/mol (Figure 3 of ref *22*). Thus, on the basis of the barrier of 17.4 kcal/mol obtained here in the mutant enzyme (Figure 2), we obtain a catalytic effect of Arg219Glu AlaR of 4.9 kcal/mol. The relative reaction free energy obtained here for the intermediate is −5.6 kcal/mol (Figure 2), suggesting an enzyme effect of 6.9 kcal/mol on Cα acidity. The effect of the mutant AlaR is contrasted with that of wt-AlaR, whose catalytic effect is obtained by comparison with the model reaction of unprotonated Ala-PLP deprotonation by phenolate in aqueous solution (*22*). The free energy barrier in wt-AlaR was found to be 7.9 kcal/mol lower than in the case of deprotonation of Ala-PLP by a phenolate ion (*19*, *22*), indicating that the wild-type enzyme has enhanced catalytic efficiency compared with the mutant enzyme value of 4.9 kcal/mol. The effect of the enzyme environment on the reaction free energy in wt-AlaR is 6.1 kcal/mol (*22*), compared with the value of 6.9 kcal/mol for the mutant enzyme, suggesting similar effects on Cα acidity.

(*ii*) *Electronic Structure Analysis*. On the basis of previous model simulations (*22*), we may suggest that the enhanced stability of the mutant intermediate is due to the electron sink ability of the pyridinium relative to the pyridine ring. This may be due to the negative charge developed in the intermediate state which is stabilized by the conjugated π system preferentially when the N1 position is protonated.

To further analyze this latter point, we performed Mülliken population analyses of the stationary points along the PMF (all values are in atomic units). Average partial charges are presented in Tables S2 and S3 of the Supporting Information. For the sake of simplicity, we will focus on the reaction progress from L-Ala-PLP to the quinonoid intermediate for the mutant AlaR and wt-AlaR, while a similar conclusion may be drawn by inspecting the reaction in the D → L direction. Moreover, to analyze charge migration, we make a virtual division of Ala-PLP along the C4−C4′ bond, into a pyridine and an Ala moiety, excluding phosphate (see Figure S2 of the Supporting Information). Inspection of the changes in the combined partial charges of these two moieties as the reaction progresses from reactant to intermediate reveals that the negative charge delocalizes mainly toward the Ala moiety. In wt-AlaR, the combined partial charge of the pyridine moiety changes from −0.90 to −1.04, while for the Ala moiety, the partial charge changes from −0.21 to −0.71. For comparison, in Arg219Glu AlaR the partial charge of the pyridine moiety changes from 0.03 to −0.06 while for the Ala moiety the partial charge changes from −0.14 to −0.72. The slightly greater delocalization into the pyridine moiety in wt-AlaR may be due to Arg219, while the presence of Glu219 might decrease the extent of such delocalization. Closer inspection of the charge partitioning in the Ala moiety between the Schiff base unit and the Cα carboxylate unit (see Figure S2 of the Supporting Information) reveals that for wt-AlaR the partial charge of the Schiff base unit changes from 0.54 to 0.34 while for the carboxylate unit it changes from −0.75 to −1.05. For comparison, in mutant AlaR, the partial charge of the Schiff base unit changes from 0.58 to 0.36, while for the carboxylate unit, the partial charge changes from −0.72 to −1.08. Thus, there is seemingly only a modest electron sink effect of the pyridine moiety in either the wild-type or the mutant enzyme, although the Ala-PLP(H^+) cofactor form slightly enhances delocalization into the Schiff base moiety.

It is of interest to compare the values given above with values obtained in the gas phase. In Ala-PLP, the partial charge of the pyridine moiety changes from −0.68 to −1.04, while for the Ala moiety, the partial charge changes from −0.32 to −0.96. In Ala-PLP(H^+), the partial charge of the pyridine moiety changes from −0.11 to −0.48, while for the Ala moiety, the partial charge changes from 0.11 to −0.52. Therefore, there is a considerable charge delocalization in the pyridine moiety both in Ala-PLP and in Ala-PLP(H^+) in the gas phase. In comparison, the extent of delocalization into the pyridine moiety is reduced considerably in both the wild-type and mutant enzymes. Indeed, in the enzyme, charge delocalization is most significant in the carboxylate

Scheme 3: Transamination Reaction in the Arg219Glu Mutant of Alanine Racemase

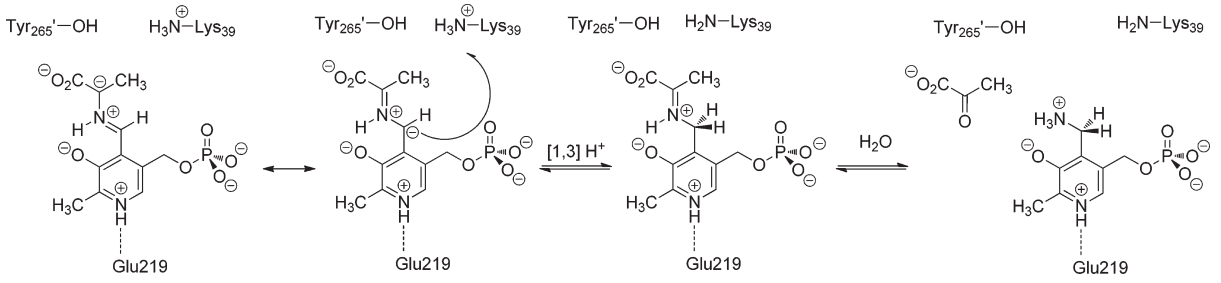

moiety, which is involved in interactions with Arg136 and the backbone amide of Met312.

(*iii*) *Structural Analysis*. The donor−acceptor distance displays typical behavior whereby the distance is gradually shortened as the reaction approaches the transition state. In the L → D half-reaction, the distance between the Ala-PLP Cα atom and the Tyr265′ oxygen is 3.11, 2.62, and 3.29 Å for the reactant, transition, and intermediate states, respectively. In the D → L half-reaction, the distance between the Ala-PLP Cα atom and the Lys39 nitrogen is 3.48, 2.71, and 3.30 Å for the reactant, transition, and intermediate states, respectively. The PLP pyridine nitrogen interacts with Glu219 via a short H-bond with average values in the reactant, transition, and intermediate states ranging from 2.55 to 2.62 Å (Tables 1 and 2). The interaction between His166 and Tyr265′ remains intact throughout the simulations, in spite of the lost interaction between His166 and Arg219 due to the mutation. The interaction between His166 and Tyr265′ in the L → D half-reaction is 2.67, 2.69, and 2.98 Å for the reactant, transition, and intermediate states, respectively. The weakening of the hydrogen bond is due to the gradual protonation of the Tyr265′ phenoxide moiety. In the opposite D → L half-reaction, the His166−Tyr265′ hydrogen bond is somewhat longer, with values of 2.83, 2.88, and 3.18 Å for the reactant, transition, and intermediate states, respectively. The interaction between Arg136 and the Ala-PLP carboxylate in the L → D half-reaction is gradually strengthened, with values of 3.71, 3.30, and 2.86 Å for the reactant, transition, and intermediate states, respectively. This significant change is due to the multiple roles played by Arg136, stabilizing the anionic Tyr265′ and the Ala-PLP carboxylate in the reactant state while in the intermediate state stabilizing more exclusively the carboxylate moiety. The interaction between Arg136 and Ala-PLP carboxylate in the D → L half-reaction is largely invariant, with values ranging from 2.59 to 2.68 Å. In this half-reaction, Tyr265′ remains protonated throughout and therefore interacts more weakly with Arg136. In conclusion, the interaction pattern observed in the Arg219-Glu mutant AlaR during racemization is similar to that in the wild-type enzyme (*22*).

Initial Stage of the Transamination Reaction. The enhanced stability of the quinonoid intermediate in Arg219Glu AlaR results in a longer lifetime for this species. The increased lifetime opens the way for potential side reactions, which would reduce the activity and specificity for racemization for this mutant. Specifically, it has been suggested that transamination of PLP to pyridoxamine 5′-phosphate (PMP), initiated by a 1,3-proton transfer from the Ala's Cα atom to C4′ of the cofactor by the Lys39 amine/ammonium group (Scheme 3), might occur (*55*−*57*). Hence, we decided to investigate the possibility of a 1,3-proton transfer in the quinonoid intermediate. Specifically, this entails the protonation of the α-pyridyl carbanion intermediate. The results shown in Figure 3 show that the barrier to reprotonation of C4′ (position α to the Schiff base) by the ammonium group of Lys39 is computed to be 18.7 kcal/mol, whereas the reprotonation barriers to the Cα atom by Lys39 and Tyr265′ are 11.6 and 23.0 kcal/mol, respectively. Hence, our simulations indicate that the 1,3-proton transfer is feasible in this mutant system and, therefore, transamination a likely side reaction in accordance with experiment. We also ascribe this to the increased stability of the quinonoid intermediate. Furthermore, in the wild-type case (Figure 4), one can see that the reprotonation barriers for the 1,1-proton transfer by Lys39 and Tyr265′ are 9.9 and 15.8 kcal/mol, respectively. These values are significantly lower than the reprotonation barrier value for the 1,3-proton transfer in the same system, which is 21.3 kcal/mol. Therefore, we also provide a rationale for the specificity of the wt-AlaR, where transamination is a less likely scenario. We note that only Lys39 was considered to be involved in the 1,3-proton transfer, although in principle Tyr265′ could also perform the same proton shuffle. Nonetheless, Lys39 is more likely to play this role because of its greater flexibility.

These results are highly significant since they suggest that the Arg219Glu mutant can catalyze other reactions in addition to the natural racemization of L/D-Ala, in contrast to the case of the wt-AlaR. This is in accordance with the experimental study by Yow et al. which showed the appearance of the characteristic absorbance peak at 300−360 nm of PMP in the Arg219Glu mutant, providing evidence for the transamination products (see Scheme 3) (*55*). Additionally, the work of Fenn et al. indicated transamination in mutant systems (*56*, *57*). Interestingly, AlaR may be engineered to provide additional functionalities, namely Tyr265′Ala, which exhibits aldolase activity (*58*, *59*). Analogously, we may compare the enzyme with D-amino acid transaminase which employs PLP as a cofactor in the conversion of D-amino acids to their corresponding α-keto acids. In this enzyme, Glu177 interacts with the pyridine nitrogen. However, it has been observed that the Glu177Lys mutant enzyme increases its racemase activity 10-fold and decreases its specific transaminase activity by more than 1000-fold (*35*). Interestingly, the crystal structure of this mutant shows that the Lys177 residue points away from the cofactor nitrogen, possibly due to electrostatic repulsion, or steric congestion due to the bulkier nature of Lys compared to Glu. This further underscores the role of this active pocket position in controlling reaction specificity.

From this analysis, we can suggest that modulating the electronic and solvation properties of the cofactor is crucial for the wt-AlaR racemization activity. Indeed, in the wild-type form, the pyridine nitrogen is unprotonated and the PLP moiety in the intermediate does not function as an electron sink (Figure 4). This destabilization of the intermediate in the wild-type system reduces the chances of side reactions, such as transamination.

Importantly, this is a direct result of the active site architecture in AlaR where the PLP pyridine nitrogen interacts with Arg219 as opposed to acidic or polar residues as in other PLP-dependent enzymes. In the Arg219Glu mutant, the stability of the Ala-PLP(H^+) cofactor is greatly enhanced, thereby increasing its lifetime and likelihood of side reactions. Analysis of the electronic distribution in the intermediate suggests that this is not primarily due to charge delocalization into the pyridine moiety, but into the Schiff base moiety and carboxylate unit. This is in accordance with the extensive work of Richard and co-workers (*32*). This may suggest a crucial role for Arg136 which interacts directly with these moieties. Additionally, the protonated cofactor reduces the total charge of the substrate−cofactor adduct, which enhances the intrinsic Cα acidity.

CONCLUSION

A key question in AlaR is the role of the PLP cofactor. We have previously shown that the main source of the catalytic effect in AlaR is enhanced solvation of the Ala-PLP moiety in the active site of AlaR (*22*). This effect was partially ascribed to the unprotonated nature of the PLP pyridine nitrogen which interacts with Arg219 in the wild-type enzyme. This conclusion contrasts earlier suggestions which indicated that the PLP cofactor serves mainly as an electron sink. The unprotonated PLP cofactor contributes 6 kcal/mol to racemization catalysis in aqueous solution (compared to Ala), whereas the enzyme environment contributes an additional 8 kcal/mol. Moreover, we found that the effect of protonation of the PLP pyridine nitrogen in aqueous solution has a catalytic effect with a >10 kcal/mol free energy barrier reduction in the absence of AlaR. This heteroatom protonation has an even stronger effect on Cα acidity in aqueous solution, which is reduced by 21 pK_a units compared to that of Ala, whereas in the unprotonated Ala-PLP, the pK_a is reduced by 13 pK_a units compared to that of Ala. In this work, we find that the enzyme is unable to significantly enhance the catalytic effect or the Cα acidity beyond the effect in water. In the Arg219Glu mutant, the stability of the Ala-PLP-(H^+) cofactor is greatly enhanced compared to that of Ala-PLP in the wild-type enzyme, thereby increasing its lifetime and the likelihood of side reactions. Analysis of the electronic distribution in the intermediate suggests that this is not primarily due to charge delocalization into the pyridine moiety, but into the Schiff base moiety and carboxylate unit, in accordance with the work of Richard and co-workers (*32*). Indeed, the principle effect of the protonated cofactor is to reduce the total charge of the substrate−cofactor adduct, which enhances the intrinsic Cα acidity.

SUPPORTING INFORMATION AVAILABLE

Tables containing partial atomic charges employed for KCX129 and Mülliken partial charge analyses and figures depicting the system setup and quantum mechanical region atom types. This material is available free of charge via the Internet at http://pubs.acs.org.

REFERENCES

1. Walsh, C. T. (1989) Enzymes in the D-alanine branch of bacterial cell wall peptidoglycan assembly. *J. Biol. Chem. 264*, 2393–2396.
2. Lam, H., Oh, D. C., Cava, F., Takacs, C. N., Clardy, J., de Pedro, M. A., and Waldor, M. K. (2009) D-Amino Acids Govern Stationary Phase Cell Wall Remodeling in Bacteria. *Science 325*, 1552–1555.
3. Mothet, J. P., Parent, A. T., Wolosker, H., Brady, R. O., Jr., Linden, D. J., Ferris, C. D., Rogawski, M. A., and Snyder, S. H. (2000) D-Serine is an endogenous ligand for the glycine site of the N-methyl-D-aspartate receptor. *Proc. Natl. Acad. Sci. U.S.A. 97*, 4926–4931.
4. Roise, D., Soda, K., Yagi, T., and Walsh, C. T. (1984) Inactivation of the *Pseudomonas striata* broad specificity amino acid racemase by D and L isomers of β-substituted alanines: Kinetics, stoichiometry, active site peptide, and mechanistic studies. *Biochemistry 23*, 5195–5201.
5. LeMagueres, P., Im, H., Dvorak, A., Strych, U., Benedik, M., and Krause, K. L. (2003) Crystal Structure at 1.45 Å Resolution of Alanine Racemase from a Pathogenic Bacterium, *Pseudomonas aeruginosa*, Contains Both Internal and External Aldimine Forms. *Biochemistry 42*, 14752–14761.
6. Badet, B., Roise, D., and Walsh, C. T. (1984) Inactivation of the dadB *Salmonella typhimurium* alanine racemase by D and L isomers of β-substituted alanines: Kinetics, stoichiometry, active site peptide sequencing, and reaction mechanism. *Biochemistry 23*, 5188–5194.
7. Esaki, N., and Walsh, C. T. (1986) Biosynthetic alanine racemase of *Salmonella typhimurium*: Purification and characterization of the enzyme encoded by the alr gene. *Biochemistry 25*, 3261–3267.
8. Badet, B., Inagaki, K., Soda, K., and Walsh, C. T. (1986) Time-dependent inhibition of *Bacillus stearothermophilus* alanine racemase by (1-aminoethyl)phosphonate isomers by isomerization to noncovalent slowly dissociating enzyme-(1-aminoethyl)phosphonate complexes. *Biochemistry 25*, 3275–3282.
9. Faraci, W. S., and Walsh, C. T. (1989) Mechanism of inactivation of alanine racemase by β,β,β-trifluoroalanine. *Biochemistry 28*, 431–437.
10. Watanabe, A., Yoshimura, T., Mikami, B., Hayashi, H., Kagamiyama, H., and Esaki, N. (2002) Reaction mechanism of alanine racemase from *Bacillus stearothermophilus* X-ray crystallographic studies of the enzyme with bound N-(5′-phosphopyridoxyl) alanine. *J. Biol. Chem. 277*, 19166–19172.
11. Amadasi, A., Bertoldi, M., Contestabile, R., Bettati, S., Cellini, B., di Salvo, M. L., Borri-Voltattorni, C., Bossa, F., and Mozzarelli, A. (2007) Pyridoxal 5′-Phosphate Enzymes as Targets for Therapeutic Agents. *Curr. Med. Chem. 14*, 1291–1324.
12. Faraci, W. S., and Walsh, C. T. (1988) Racemization of alanine by the alanine racemases from *Salmonella typhimurium* and *Bacillus stearothermophilus*: Energetic reaction profiles. *Biochemistry 27*, 3267–3276.
13. Shaw, J. P., Petsko, G. A., and Ringe, D. (1997) Determination of the Structure of Alanine Racemase from *Bacillus stearothermophilus* at 1.9-Å Resolution. *Biochemistry 36*, 1329–1342.
14. Stamper, C. G. F., Morollo, A. A., and Ringe, D. (1998) Reaction of Alanine Racemase with 1-Aminoethylphosphonic Acid Forms a Stable External Aldimine. *Biochemistry 37*, 10438–10445.
15. Sun, S., and Toney, M. D. (1999) Evidence for a Two-Base Mechanism Involving Tyrosine-265 from Arginine-219 Mutants of Alanine Racemase. *Biochemistry 38*, 4058–4065.
16. Watanabe, A., Yoshimura, T., Mikami, B., and Esaki, N. (1999) Tyrosine 265 of alanine racemase serves as a base abstracting α-hydrogen from L-alanine: The counterpart residue to lysine 39 specific to D-alanine. *J. Biochem. 126*, 781.
17. Watanabe, A., Kurokawa, Y., Yoshimura, T., Kurihara, T., Soda, K., and Esaki, N. (1999) Role of lysine 39 of alanine racemase from *Bacillus stearothermophilus* that binds pyridoxal 5′-phosphate. Chemical rescue studies of Lys39 → Ala mutant. *J. Biol. Chem. 274*, 4189–4194.
18. Spies, M. A., and Toney, M. D. (2003) Multiple Hydrogen Kinetic Isotope Effects for Enzymes Catalyzing Exchange with Solvent: Application to Alanine Racemase. *Biochemistry 42*, 5099–5107.
19. Spies, M. A., Woodward, J. J., Watnik, M. R., and Toney, M. D. (2004) Alanine Racemase Free Energy Profiles from Global Analyses of Progress Curves. *J. Am. Chem. Soc. 126*, 7464–7475.
20. Spies, M. A., and Toney, M. D. (2007) Intrinsic primary and secondary hydrogen kinetic isotope effects for alanine racemase from global analysis of progress curves. *J. Am. Chem. Soc. 129*, 10678–10685.
21. Major, D. T., Nam, K., and Gao, J. (2006) Transition State Stabilization and α-Amino Carbon Acidity in Alanine Racemase. *J. Am. Chem. Soc. 128*, 8114–8115.
22. Major, D. T., and Gao, J. (2006) A Combined Quantum Mechanical and Molecular Mechanical Study of the Reaction Mechanism and α-Amino Acidity in Alanine Racemase. *J. Am. Chem. Soc. 128*, 16345–16357.
23. Dixon, J. E., and Bruice, T. C. (1973) Comparison of the rate constants for general base catalyzed prototropy and racemization of the aldimine species formed from 3-hydroxypyridine-4-carboxaldehyde and alanine. *Biochemistry 12*, 4762–4766.
24. Toney, M. D. (2005) Reaction specificity in pyridoxal phosphate enzymes. *Arch. Biochem. Biophys. 433*, 279–287.

25. Sharif, S., Huot, M. C., Tolstoy, P. M., Toney, M. D., Jonsson, K. H. M., and Limbach, H. H. (2007) ^{15}N nuclear magnetic resonance studies of acid-base properties of pyridoxal-5′-phosphate aldimines in aqueous solution. *J. Phys. Chem. B 111*, 3869–3876.
26. McPhalen, C. A., Vincent, M. G., and Jansonius, J. N. (1992) X-ray Structure Refinement and Comparison of Three Forms of Mitochondrial Aspartate Aminotransferase. *J. Mol. Biol. 225*, 495–517.
27. Hyde, C. C., Ahmed, S. A., Padlan, E. A., Miles, E. W., and Davies, D. R. (1988) Three-dimensional Structure of the Tryptophan Synthase a2b2 Multienzyme Complex from *Salmonella typhimurium*. *J. Biol. Chem. 263*, 17857–17871.
28. Bach, R. D., and Canepa, C. (1997) Theoretical model for pyruvoyl-dependent enzymatic decarboxylation of α-amino acids. *J. Am. Chem. Soc. 119*, 11725–11733.
29. Bach, R. D., Canepa, C., and Glukhovtsev, M. N. (1999) Influence of electrostatic effects on activation barriers in enzymatic reactions: Pyridoxal 5′-phosphate-dependent decarboxylation of α-amino acids. *J. Am. Chem. Soc. 121*, 6542–6555.
30. Jencks, W. P., and Regenstein, J. (1976) Ionization constants of acids and bases, Vol. *1*, CRC Press, Boca Raton, FL.
31. Toth, K., and Richard, J. P. (2007) Covalent Catalysis by Pyridoxal: Evaluation of the Effect of the Cofactor on the Carbon Acidity of Glycine. *J. Am. Chem. Soc. 129*, 3013–3021.
32. Richard, J. P., Amyes, T. L., Crugeiras, J., and Rios, A. (2009) Pyridoxal 5′-phosphate: Electrophilic catalyst extraordinaire. *Curr. Opin. Chem. Biol. 13*, 475–483.
33. Rubinstein, A., and Major, D. T. (2009) Catalyzing racemizations in the absence of a cofactor: The reaction mechanism in proline racemase. *J. Am. Chem. Soc. 131*, 8513–8521.
34. Brooks, B. R., Bruccoleri, R. E., Olafson, B. D., States, D. J., Swaminathan, S., and Karplus, M. (1983) CHARMM: A program for macromolecular energy, minimization, and dynamics calculations. *J. Comput. Chem. 4*, 187–217.
35. van Ophem, P. W., Peisach, D., Erickson, S. D., Soda, K., Ringe, D., and Manning, J. M. (1999) Effects of the E177K Mutation in D-Amino Acid Transaminase. Studies on an Essential Coenzyme Anchoring Group That Contributes to Stereochemical Fidelity. *Biochemistry 38*, 1323–1331.
36. Sharif, S., Schagen, D., Toney, M. D., and Limbach, H. H. (2007) Coupling of functional hydrogen bonds in pyridoxal-5′-phosphate-enzyme systems observed by solid-state NMR spectroscopy. *J. Am. Chem. Soc. 129*, 4440–4455.
37. Sharif, S., Fogle, E., Toney, M. D., Denisov, G. S., Shenderovich, I. G., Buntkowsky, G., Tolstoy, P. M., Huot, M. C., and Limbach, H. H. (2007) NMR localization of protons in critical enzyme hydrogen bonds. *J. Am. Chem. Soc. 129*, 9558–9559.
38. Sharif, S., Denisov, G. S., Toney, M. D., and Limbach, H. H. (2007) NMR Studies of Coupled Low- and High-Barrier Hydrogen Bonds in Pyridoxal-5′-phosphate Model Systems in Polar Solution. *J. Am. Chem. Soc. 129*, 6313–6327.
39. Gao, J. (1995) in Methods and Applications of Combined Quantum Mechanical and Molecular Mechanical Potentials, (Lipkowitz, K. B., and Boyd, D. B., Eds) Vol. *7*, pp 119−185, VCH Publishers, New York.
40. Puig, E., Mixcoha, E., Garcia-Viloca, M., Gonzalez-Lafont, A., and Lluch, J. M. (2009) How the substrate D-glutamate drives the catalytic action of *Bacillus subtilis* glutamate racemase. *J. Am. Chem. Soc. 131*, 3509–3521.
41. MacKerell, A. D., Jr., Bashford, D., Bellott, M., Dunbrack, R. L., Jr., Evanseck, J. D., Field, M. J., Fischer, S., Gao, J., Guo, H., Ha, S., Joseph-McCarthy, D., Kuchnir, L., Kuczera, K., Lau, F. T. K., Mattos, C., Michnick, S., Ngo, T., Nguyen, D. T., Prodhom, B., Reiher, W. E., III, Roux, B., Schlenkrich, M., Smith, J. C., Stote, R., Straub, J., Watanabe, M., Wiorkiewicz-Kuczera, J., Yin, D., and Karplus, M. (1998) All-Atom Empirical Potential for Molecular Modeling and Dynamics Studies of Proteins. *J. Phys. Chem. B 102*, 3586–3616.
42. Foloppe, N., and MacKerell, A. D., Jr. (2000) All-Atom Empirical Force Field for Nucleic Acids: 1) Parameter Optimization Based on Small Molecule and Condensed Phase Macromolecular Target Data. *J. Comput. Chem. 21*, 86–104.
43. MacKerell, A. D., Jr., and Banavali, N. (2000) All-Atom Empirical Force Field for Nucleic Acids: 2) Application to Molecular Dynamics Simulations of DNA and RNA in Solution. *J. Comput. Chem. 21*, 105–120.
44. Jorgensen, W. L., Chandrasekhar, J., Madura, J. D., Impey, R. W., and Klein, M. L. (1983) Comparison of simple potential functions for simulating liquid water. *J. Chem. Phys. 79*, 926–935.
45. Kottalam, J., and Case, D. A. (1988) Dynamics of ligand escape from the heme pocket of myoglobin. *J. Am. Chem. Soc. 110*, 7690–7697.
46. Torrie, G. M., and Valleau, J. P. (1977) Nonphysical sampling distributions in Monte Carlo free-energy estimation: Umbrella sampling. *J. Comput. Phys. 23*, 187–199.
47. Kumar, S., Rosenberg, J. M., Bouzida, D., Swendsen, R. H., and Kollman, P. A. (1992) The weighted histogram analysis method for free-energy calculations on biomolecules. I. The method. *J. Comput. Chem. 13*, 1011–1021.
48. Brunger, A., Brooks, C. L., III, and Karplus, M. (1984) Stochastic boundary conditions for molecular dynamics simulations of ST2 water. *Chem. Phys. Lett. 105*, 495–500.
49. Brooks, C. L., III, Brunger, A., and Karplus, M. (1985) Active site dynamics in protein molecules: A stochastic boundary molecular-dynamics approach. *Biopolymers 24*, 843–865.
50. Allen, M. P., and Tildesley, D. J. (1990) Computer simulation of liquids, Oxford University Press, New York.
51. Northrup, S. H., Pear, M. R., Lee, C. Y., McCammon, J. A., and Karplus, M. (1982) Dynamical theory of activated processes in globular proteins. *Proc. Natl. Acad. Sci. U.S.A. 79*, 4035–4039.
52. Major, D. T., and Gao, J. (2005) Implementation of the bisection sampling method in path integral simulations. *J. Mol. Graphics Modell. 24*, 121–127.
53. Major, D. T., Garcia-Viloca, M., and Gao, J. (2006) Path Integral Simulations of Proton Transfer Reactions in Aqueous Solution Using Combined QM/MM Potentials. *J. Chem. Theory Comput. 2*, 236–245.
54. Major, D. T., and Gao, J. (2007) An Integrated Path Integral and Free-Energy Perturbation Umbrella Sampling Method for Computing Kinetic Isotope Effects of Chemical Reactions in Solution and in Enzymes. *J. Chem. Theory Comput. 3*, 949–960.
55. Yow, G. Y., Watanabe, A., Yoshimura, T., and Esaki, N. (2003) Conversion of the catalytic specificity of alanine racemase to a D-amino acid aminotransferase activity by a double active-site mutation. *J. Mol. Catal. B: Enzym. 23*, 311–319.
56. Fenn, T. D., Stamper, G. F., Morollo, A. A., and Ringe, D. (2003) A Side Reaction of Alanine Racemase: Transamination of Cycloserine. *Biochemistry 42*, 5775–5783.
57. Fenn, T. D., Holyoak, T., Stamper, G. F., and Ringe, D. (2005) Effect of a Y265F Mutant on the Transamination-Based Cycloserine Inactivation of Alanine Racemase. *Biochemistry 44*, 5317–5327.
58. Seebeck, F. P., and Hilvert, D. (2003) Conversion of a PLP-Dependent Racemase into an Aldolase by a Single Active Site Mutation. *J. Am. Chem. Soc. 125*, 10158–10159.
59. Seebeck, F. P., Guainazzi, A., Amoreira, C., Baldridge, K. K., and Hilvert, D. (2006) Stereoselectivity and Expanded Substrate Scope of an Engineered PLP-Dependent Aldolase. *Angew. Chem., Int. Ed. 45*, 6824–6826.